Theoretical and experimental investigation of magnetoelectric effect for bending-tension coupled modes in magnetostrictive-piezoelectric layered composites

D. Hasanyan, J. Gao, Y. Wang, R. Viswan, M. Li, Y. Shen, J. Li, and D. Viehland

Articles you may be interested in

The effects of interface misfit strain and surface tension on magnetoelectric effects in layered magnetostrictive-piezoelectric composites
J. Appl. Phys. 114, 044109 (2013); 10.1063/1.4816693

Highly zero-biased magnetoelectric response in magnetostrictive/piezoelectric composite
J. Appl. Phys. 112, 024504 (2012); 10.1063/1.4737404

Theory of magnetoelectric effect for bending modes in magnetostrictive-piezoelectric bilayers
J. Appl. Phys. 105, 063911 (2009); 10.1063/1.3087766

Large high-frequency magnetoelectric response in laminated composites of piezoelectric ceramics, rare-earth iron alloys and polymer
Appl. Phys. Lett. 84, 3516 (2004); 10.1063/1.1739277

Characterization of magnetoelectric laminate composites operated in longitudinal-transverse and transverse–transverse modes
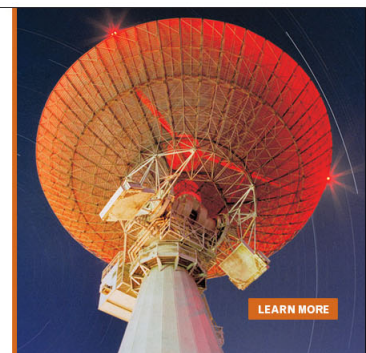J. Appl. Phys. 95, 2625 (2004); 10.1063/1.1644027

Theoretical and experimental investigation of magnetoelectric effect for bending-tension coupled modes in magnetostrictive-piezoelectric layered composites

D. Hasanyan,[a] J. Gao, Y. Wang, R. Viswan, M. Li, Y. Shen, J. Li, and D. Viehland

Materials Science and Engineering, Virginia Tech, Blacksburg, Virginia 24061, USA

In this paper, we discuss a theoretical model with experimental verification for the resonance enhancement of magnetoelectric (ME) interactions at frequencies corresponding to bending-tension oscillations. A dynamic theory of arbitrary laminated magneto-elasto-electric bars was constructed. The model included bending and longitudinal vibration effects for predicting ME coefficients in laminate bar composite structures consisting of magnetostrictive, piezoelectric, and pure elastic layers. The thickness dependence of stress, strain, and magnetic and electric fields within a sample are taken into account, as such the bending deformations should be considered in an applied magnetic or electric field. The frequency dependence of the ME voltage coefficients has obtained by solving electrostatic, magnetostatic, and elastodynamic equations. We consider boundary conditions corresponding to free vibrations at both ends. As a demonstration, our theory for multilayer ME composites was then applied to ferromagnetic-ferroelectric bilayers, specifically Metglas-PZT ones. A theoretical model is presented for static (low-frequency) ME effects in such bilayers. We also performed experiments for these Metglas-PZT bilayers and analyzed the influence of Metglas geometry (length and thickness) and Metglas/PZT volume fraction on the ME coefficient. The frequency dependence of the ME coefficient is also presented for different geometries (length, thickness) of Metglas. The theory shows good agreement with experimental data, even near the resonance frequency. © *2012 American Institute of Physics*. [http://dx.doi.org/10.1063/1.4732130]

I. INTRODUCTION

Active materials with coupled electric, magnetic, and elastic parameters that simultaneously display ferroelectricity, ferromagnetism, and ferroelasticity can be called multiferroics. Multiferroics are a special class of materials that have attracted much attention because of their potential for enhanced functionality in sensors and other devices.[1–3] Magnetoelectric (ME) effects are defined as an induced polarization in an applied magnetic field, or an induced magnetization in an applied electric field. The ME effect is studied by subjecting the sample to a magnetic (electric) bias field and an ac magnetic field. One then measures the resulting ac electric (magnetic) field produced in the material. Over the past fifty years, ME materials have evolved from single phase compounds, to particulate composites, and finally to laminate composites.[1–4] Remarkably higher ME effects observed in laminate composites are produced by mechanically coupling continuous magnetostrictive and piezoelectric layers. While several models for laminate ME composites exist, these significantly over predict the experimental results.[1–4] Here, we provide an explanation for this discrepancy, and a corresponding analytical model that corrects these differences which is validated with experimental results.

Prior modeling investigations of laminate ME composites have sometimes made questionable assumptions: for example, a homogeneous distribution of field functions (stress, strain, and electromagnetic) through the layers. Based on these approaches, many authors[1–4] have provided an analytical foundation for static ME laminate composites. However, these theoretical approaches have yielded a huge disagreement with experiments, because of an assumption that all field functions are homogeneously distributed throughout the composite. To eliminate disagreement between analysis and experiments, various authors[2–5] have proposed a model that was free of the above mentioned assumption, where field functions were allowed to vary along (only) the longitudinal direction of the laminates (i.e., no bending). While this provided an approach to better correlate theoretical analysis with experimental data, the approach was applicable only to symmetric laminated composite structures. However, for nonsymmetrical structures, this model remained questionable. For example, ferromagnetic-ferroelectric bilayers cannot be modeled only with interactions along the longitudinal direction: in this particular case, bending-tension modes always couple together and the field functions vary not only along the longitudinal direction but also through the thickness as well. Please note that the mechanism of ferromagnetic-ferroelectric interactions in this case is quite complicated and that simplified approaches to describe them often do not provide adequate conclusions.

Since the ME coupling in composites is directly produced by the mechanical stress, one would expect orders of magnitude stronger coupling when the frequency of the ac field is tuned to acoustic mode frequencies in the sample, relative to non-resonance ones. Many recent experiments and modeling efforts have dealt with ME interactions at

---

[a] Author to whom correspondence should be addressed. Electronic mail: davreshh@yahoo.com.

112, 013908-1

electromechanical resonances in layered composites.[4] However, a key drawback of these studies of ME resonance effects was that the resonance frequencies were quite high, on the order of hundreds of kilohertz for nominal samples of normal dimensions. In order to reduce the resonance frequency, researchers have increased the laminate size, which is disadvantageous for many applications. An alternative approach to achieving strong ME coupling at lower frequencies is resonance enhancement using bending modes of the composite. The frequency of ac fields that must be applied to the composite for such bending oscillations is much lower than that of the longitudinal acoustic modes. Recent investigations have shown giant ME effects at bending modes in several layered structures.[6–16]

Here, we focus our attention on developing a model which describes the dynamic ME effects at bending-tension coupled modes. The important aspects of the model are as follows: the thickness dependence of stress, strain, and magnetic and electric fields within a sample are taken into account so that the bending deformations of a multilayer composite in an applied magnetic or electric field can be considered. For simplicity, we developed a model for a multilayer beam-plate structure. Many papers have been devoted to symmetrically and asymmetrically laminated electroelastic bars: a bar theory, as a rule, is constructed by the method of hypotheses.[17,18] In this case, the well-known Kirchhoff's hypotheses are used for the mechanical quantities. The hypotheses for the electrical quantities are generally taken without considering the electrical boundary conditions of the faces of the piezoelectric-piezomagnetic layers.

As a validation, the theory that we developed for multilayer ME composites was applied to ferromagnetic-ferroelectric bilayers. We considered boundary conditions corresponding to free vibrations at both ends. Frequency dependent longitudinal and transverse ME voltage coefficients were obtained using the simultaneous solutions to the electrostatic, magnetostatic, and elastodynamic equations. The ME voltage coefficients were estimated from known material parameters and were then compared to experimental data for bilayers. The model is applied to the specific case of Metglas-PZT bilayers. A theoretical model is presented for static (low-frequency) ME effects in bilayers as a particular case. We analyzed the influence of Metglas geometry (length and thickness) and Metglas/PZT volume fraction on ME coefficient. We also performed experiments for Metglas-PZT bilayers. The frequency dependence of the ME coefficient is presented for different geometries (length and thickness) of Metglas. The theory shows good agreement with experimental data even around resonance frequency.

II. MODEL AND CONSTITUITIVE EQUATIONS FOR A MULTI-LAYER ME LAMINATE COMPOSITE

Consider an arbitrary laminated structure of length $2L$ and N layers. In this case, there is no middle plane of the bar that can serve as a plane of symmetry. For simplicity, we will assume that the multilayer structure is two dimensional (i.e., a bar structure). In this case, the field functions depend only on the space coordinates x_1 and x_3. The geometry and the magnetic loads are represented schematically in Fig. 1. The x_1 axis in Cartesian coordinates is directed along the bar length, the x_2 axis is directed across the width, and the x_3 axis is orthogonal to them both. It is assumed that the piezoelectric layers are poled in the x_1 direction. It should be mentioned that the proposed theory can be successfully applied to multilayer structures when the polarization direction of the piezoelectric layers is along the x_3 direction, or when some of them are along x_1 and along x_3 or x_2.

We then assumed that the total thickness of the multilayers can be given by

$$h = \sum_{k=1}^{N} h_k = \sum_{k=1}^{N_p} h_{kp} + \sum_{k=1}^{N_m} h_{km} + \sum_{k=1}^{N_e} h_{ke}, \quad (1)$$

where $N = N_P + N_M + N_E$ is the total number of layers; N_P is the number of ferroelectric layers; N_M is the number of ferromagnetic layers; N_E is the number of pure elastic ones; h_k ($k = 1, N$) is the thickness of the kth layer; h_{kP} ($k = 1, N_P$) is the thickness of the ferroelectric kth layer; h_{kM} ($k = 1, N_M$) is the thickness of the ferromagnetic kth layer; and h_{kE} ($k = 1, N_E$) is the thickness of the elastic kth layer. Later, we will use the following notations as well: $H_p = \sum_{k=1}^{N_p} h_{kp}$ which is the total thickness of the piezoelectric layers, $H_M = \sum_{k=1}^{N_M} h_{kM}$ which is the total thickness of the piezomagnetic layers, $H_E = \sum_{k=1}^{N_e} h_{ke}$ which is the total thickness of the elastic layers, and $H = h = Hp + H_M + H_E$ which is the total thickness of the composite (Fig. 2).

A. Basic assumptions and restrictions

We then make the following assumptions and restrictions:

(I)   The layers are perfectly bonded together (i.e., no cracks or other type of imperfections).
(II)   The Material of each layer is linearly elastic.
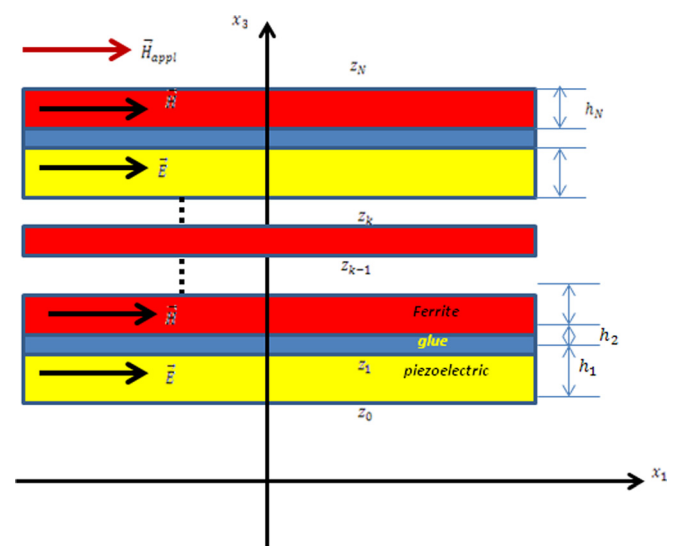(III) Each layer is of uniform thickness.

FIG. 1. Magneto electric multilayer laminated composite. The arrows indicate the direction of polarization in piezoelectric layer, applied magnetic field and induced magnetic field in ferromagnetic layer.
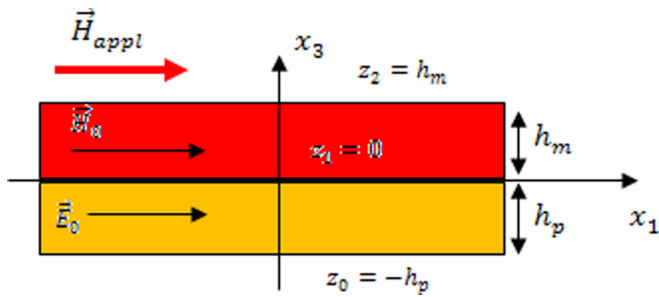
FIG. 2. Piezomagnetic-piezoelectric bi-layer in an applied magnetic field.

(IV)   The strains and displacements are small.
(V)   The length of the composite is much greater than the total thickness, i.e., $L \gg h$.
(VI)   The transverse shear stresses on the top and bottom surfaces of the laminate are zero.
(VII)   Bernoulli's (Kirchhoff's) hypothesis are valid for any layer, i.e., the displacements in x_1 and x_3 directions can be given as

$$\begin{cases} u_1(x_1, x_3) = u(x_1) - x_3 \dfrac{\partial w}{\partial x_1}, \\ u_3(x_1, x_3) = w(x_1) \end{cases} \quad (2)$$

where $u(x_1)$ and $w(x_1)$ are plates midplane displacements in x_1 and x_3 directions, respectively.

We also assume that the specimen was poled along the longitudinal (L) direction (i.e., x_1-axis). The dc and ac magnetic fields were then applied along the L direction and across

the planes of the contacts ($\vec{H}_{appl}$). The magnetostrictive and piezoelectric layers were assumed to be bonded together with an elastic bonding material-layer of a finite thickness.

Due to magnetostriction, an alternating magnetic field induces vibrations in the magnetostrictive layers, which propagates both across and along the specimen. Mechanical vibrations of the ferrite medium are transferred to the piezoelectric component, via mechanical bonding, wherein an electric field is induced by the piezoelectric effect. Our further considerations will be a case of coupled bending and longitudinal vibrations of this multilayer structure.

With the above assumptions of (I) to (VII), the equations of motions and Maxwell's electro-magneto static equations, the elastic, magnetic and electro elastic layers can be written as follows (see Refs. 17–20)

$$T_{ij,i}^{(k)} = \rho_k > \frac{\partial^2 u_j^{(k)}}{\partial t^2} \ (k = 1, 2, \ldots, N) \quad (3)$$

$$B_{i,i}^{(k)} = 0, \quad e_{ijm}H_{j,m}^{(k)} = 0 \ (k = 1, 2, \ldots, N) \quad (4)$$

$$D_{i,i}^{(k)} = 0, \quad e_{ij,m}E_{j,m}^{(k)} = 0, \ (k = 1, 2, \ldots, N); \quad (5)$$

where $F_{,i} = \frac{\partial F}{\partial x_i}$; e_{ijm} is the permutation symbol with $e_{ijm} = 1$ or -1 depending on whether the indices are in cyclic or anti-cyclic order, respectively, and $e_{ijm} = 0$; otherwise, the superscript in parentheses denotes the number of the layer. The constitutive equations for the magnetostrictive, piezoelectric and pure elastic layers can then be expressed in the following forms (see Refs. 6, 18–20):

Piezoelectric media

$$\begin{cases} S_{iP}^{(k)} = s_{Pij}^{(k)}T_{jP}^{(k)} + d_{mi}^{(k)}E_m^{(k)} \\ D_{mP}^{(k)} = d_{mi}^{(k)}T_{iP}^{(k)} + \varepsilon_{mn}^{(k)}E_n^{(k)} \end{cases} \quad (k = 1, 2, \ldots, N_P; \ i, j = 1, \ldots, 6; \ m, n = 1, 2, 3); \quad (6)$$

Magnetostrictive media

$$\begin{cases} S_{iM}^{(k)} = s_{Mij}^{(k)}T_{jM}^{(k)} + q_{mi}^{(k)}H_m^{(k)} \\ B_{mM}^{(k)} = q_{mi}^{(k)}T_{iM}^{(k)} + \mu_{mn}^{(k)}H_n^{(k)} \end{cases} \quad (k = 1, 2, \ldots, N_M; \ i, j = 1, \ldots, 6; \ m, n = 1, 2, 3); \quad (7)$$

Pure elastic media

$$S_{iE}^{(k)} = s_{Eij}^{(k)}T_{jE}^{(k)} \quad (k = 1, 2, \ldots, N_E; \ i, j = 1, \ldots, 6). \quad (8)$$

In Eqs. (6)–(8), we introduced the following notations: S_i and T_i are the strain and stress tensor components; E_m and D_m are the vector components of electric field and displacement; H_m and B_m are the vector components of magnetic field and induction; $S_{Pij}^{(k)}$, $S_{Mij}^{(k)}$ and $S_{Eij}^{(k)}$ are the compliance matrixes of the piezoelectric, piezomagnetic, and pure elastic media, respectively; q_{mi} and d_{mi} are the piezomagnetic and piezoelectric coefficients; ε_{km} and μ_{km} are the dielectric permittivity and magnetic permeability matrixes, respectively.

The sub indexes P, M, and E correspond to the piezoelectric and piezomagnetic phases and substrate (i.e., pure elastic media), respectively, where the superscripts in the parentheses denote the number of the layer. If the material of the layer is not specified then for compliances we will use notation $S_{ij}^{(k)}$. We assume that the symmetry of the piezoelectric phase is ∞m and that of the piezomagnetic one is cubic.

As in elastic bar theory,[17,18] the stresses T_2 and T_3 in the constitutive relations can be neglected compared to the stress T_1, and it is assumed that the magneto-electro-elastic state does not depend on the x_2 coordinate. Within the scope of Bernoulli's (Kirchhoff's) hypothesis of beam bending theory, only the strain S_1 is induced in a beam, given as

$$S_1 = \frac{\partial u_1(x_1, x_3)}{\partial x_1} = \frac{\partial u(x_1)}{\partial x_1} - x_3 \frac{\partial^2 w}{\partial x_1^2} = \varepsilon - x_3 \kappa; \quad (9)$$

where $\varepsilon = \frac{\partial u(x_1)}{\partial x_1}$ is a strain along the neutral axis and $\kappa = \frac{\partial^2 w}{\partial x_1^2}$ is a bending of the neutral axis. Equation (9) denotes the linear behavior of the strain S_1 over the entire cross section of the bending beam, whereas x_3 defines the distance from the neutral axis.

B. Boundary conditions on the interfaces of layers

We next provide the most frequently used boundary conditions for the electrical quantities. If there are no electrodes on the surfaces of the bar and the layer on their surfaces is in contact with a non-conducting medium (i.e., insulating glue or a vacuum or air), the component of the electric induction vector D_3 normal to these surfaces equals zero:

$$D_3 = 0. \quad (10)$$

For the electrical field, magnetic field, and magnetic induction components, the following boundary conditions should be satisfied

$$E_1^{(k)}\Big|_{x_3=z_k} = E_1^{(k+1)}\Big|_{x_3=z_k}; \quad H_1^{(k)}\Big|_{x_3=z_k} = H_1^{(k+1)}\Big|_{x_3=z_k};$$

$$B_3^{(k)}\Big|_{x_3=z_k} = B_3^{(k+1)}\Big|_{x_3=z_k}; \quad (11)$$

where $(k = 0, 1, \ldots N+1)$ and the components with "0" or "N + 1" superscript in parentheses indicate electromagnetic components with surrounding area to the laminate. If the electrodes are in open-circuit conditions, then the following integral condition for the current is satisfied

$$I = \iint_S \frac{dD_1}{dt} ds = i\omega \iint_S D_1 ds = 0, \quad (12)$$

where the integral is evaluated over the surface S of electrodes.

The mechanical load on the surface is given that on the bar faces, namely

$$T_6^{(N)}\Big|_{x_3=z_N} = q_1^+; \quad T_6^{(N)}\Big|_{x_3=z_0} = q_1^-; \quad (13)$$

$$T_3^{(N)}\Big|_{x_3=z_N} = q_3^+; \quad T_3^{(N)}\Big|_{x_3=z_0} = q_3^-; \quad (14)$$

where $q_i^\pm$ are the forces applied on the surfaces $x_3 = z_N$ and $x_3 = z_0$. The boundary conditions on the composite edges should also be included as well. We will provide these conditions later in a paragraph related to vibration of multilayer composites.

In order to construct a theory of ME bars, some additional assumptions regarding the electrical and magnetic quantities must be made. As in the theory of piezoelectric shells and plates,[17–21] the content of the hypotheses assumed depends on the electrical conditions on the surfaces of the ME layers. For the piezoelectric layers, we will make the following assumptions, which were previously justified by an asymptotic method for single-layer electro elastic plates and shells:[17–21]

- The electric field component $E_1^{(k)}(x_1, x_3)$ is not a function of the thickness coordinate x_3, i.e.

$$E_1^{(k)}(x_1, x_3) = E_0^{(k)}(x_1) = E_0(x_1). \quad (15)$$

- The magnetic field component $H_1^{(k)}(x_1, x_3)$ is not a function of the thickness coordinate x_3, i.e.

$$H_1^{(k)}(x_1, x_3) = H_0^{(k)}(x_1) = H_0(x_1). \quad (16)$$

- The third component of magnetic induction is zero, i.e.

$$B_3^{(k)}(x_1, x_3) \equiv 0. \quad (17)$$

Note that due to assumptions (15)–(17) that the boundary conditions given in Eq. (11) are automatically fulfilled. These three assumptions can be derived by the asymptotic integration of Maxwell's equations (4) and (5) in composite layers and surrounding areas. These assumptions are the first terms in an asymptotic representation. Any further foundation of assumptions (15)–(17) are outside of the scope of this paper. Analogous asymptotic integration of Maxwell's equations for only piezoelectric layers was provided in Refs. 17–21.

III. RESULTING TANGENTIAL FORCE AND BENDING MOMENT

Due to representation (9), the induced stresses in the kth layers of the various phases can be expressed as

Piezoelectric layer

$$T_{1P}^{(k)} = \frac{1}{s_{P11}^{(k)}} \left(\varepsilon - x_3 \kappa - d_{11}^{(k)} E_1^{(k)} \right) \quad (k = 1, 2 \ldots N_P). \quad (18)$$

Piezomagnetic layer

$$T_{1M}^{(k)} = \frac{1}{s_{M11}^{(k)}} \left(\varepsilon - x_3 \kappa - q_{11}^{(k)} H_1^{(k)} \right) \quad (k = 1, 2 \ldots N_M). \quad (19)$$

Elastic layer

$$T_{1E}^{(k)} = \frac{1}{s_{E11}^{(k)}} \left(\varepsilon - x_3 \kappa \right) \quad (k = 1, 2 \ldots N_E). \quad (20)$$

By integrating the stresses over the thickness, we can obtain the resultant tangential force T_1 in the following form

$$T_1 = \sum_{k=1}^{N} \int_{z_{k-1}}^{z_k} T_1^{(k)}(x_1, x_3) dx_3$$

$$= \sum_{k=1}^{N_P} \int_{z_{k-1}^P}^{z_k^P} T_{1P}^{(k)}(x_1, x_3) dx_3$$

$$+ \sum_{k=1}^{N_M} \int_{z_{k-1}^M}^{z_k^M} T_{1M}^{(k)}(x_1, x_3) dx_3$$

$$+ \sum_{k=1}^{N_E} \int_{z_{k-1}^E}^{z_k^E} T_{1E}^{(k)}(x_1, x_3) dx_3. \quad (21)$$

Using Eqs. (18)–(20), the expression in Eq. (21) for T_1 results in

$$T_1 = A\varepsilon - B\kappa - A_{01}E_0 - A_{02}H_0, \tag{22}$$

where

$$A = \sum_{k=1}^{N_P} \frac{h_{kP}}{s_{P11}^{(k)}} + \sum_{k=1}^{N_M} \frac{h_{kM}}{s_{M11}^{(k)}} + \sum_{k=1}^{N_E} \frac{h_{kE}}{s_{E11}^{(k)}},$$

$$B = \sum_{k=1}^{N_P} \frac{1}{2s_{P11}^{(k)}} \left[(z_k^P)^2 - (z_{k-1}^P)^2 \right] + \sum_{k=1}^{N_M} \frac{1}{2s_{M11}^{(k)}}$$

$$\left[(z_k^M)^2 - (z_{k-1}^M)^2 \right] + \sum_{k=1}^{N_E} \frac{1}{2s_{E11}^{(k)}} \left[(z_k^E)^2 - (z_{k-1}^E)^2 \right],$$

$$A_{01} = \sum_{k=1}^{N_P} \frac{d_{11}^{(k)} h_{kP}}{s_{P11}^{(k)}}, \quad A_{02} = \sum_{k=1}^{N_P} \frac{q_{11}^{(k)} h_{kM}}{s_{M11}^{(k)}}. \tag{23}$$

The resulting bending moment M_1 is calculated according to

$$M_1 = \sum_{k=1}^{N} \int_{z_{k-1}}^{z_k} x_3 T_1^{(k)}(x_1, x_3) dx_3$$

$$= \sum_{k=1}^{N_P} \int_{z_{k-1}^P}^{z_k^P} x_3 T_{1P}^{(k)}(x_1, x_3) dx_3$$

$$+ \sum_{k=1}^{N_M} \int_{z_{k-1}^M}^{z_k^M} x_3 T_{1M}^{(k)}(x_1, x_3) dx_3$$

$$+ \sum_{k=1}^{N_E} \int_{z_{k-1}^E}^{z_k^E} x_3 T_{1E}^{(k)}(x_1, x_3) dx_3. \tag{24}$$

Using Eqs. (18)–(20), the expression in Eq. (24) for M_1 results in

$$M_1 = B\varepsilon - D\kappa - C_1 E_0 - C_2 H_0; \tag{25}$$

where

$$D = \sum_{k=1}^{N_P} \frac{1}{3s_{P11}^{(k)}} \left[(z_k^P)^3 - (z_{k-1}^P)^3 \right] + \sum_{k=1}^{N_M} \frac{1}{3s_{M11}^{(k)}}$$

$$\left[(z_k^M)^3 - (z_{k-1}^M)^3 \right] + \sum_{k=1}^{N_E} \frac{1}{3s_{E11}^{(k)}} \left[(z_k^E)^3 - (z_{k-1}^E)^3 \right] \tag{26}$$

$$C_1 = \sum_{k=1}^{N_P} \frac{d_{11}^{(k)}}{2s_{P11}^{(k)}} \left[(z_k^P)^2 - (z_{k-1}^P)^2 \right],$$

$$C_2 = \sum_{k=1}^{N_M} \frac{q_{11}^{(k)}}{2s_{M11}^{(k)}} \left[(z_k^M)^2 - (z_{k-1}^M)^2 \right]. \tag{27}$$

In the context of the above simplification, from the second equation in Eq. (6), the component of electric displacement D_1 can be expressed in a following form

$$D_1 = \sum_{k=1}^{N_P} \int_{z_{k-1}^P}^{z_k^P} D_1^{(k)}(x_1, x_3) dx_3. \tag{28}$$

Using Eqs. (18)–(20), the expression (28) results in

$$C_3 E_0 + C_4 \varepsilon - C_5 \kappa = D_1; \tag{29}$$

where

$$C_3 = \sum_{k=1}^{N_P} \varepsilon_{11}^{(k)} (1 - K_{1k}^2) h_{kP}, \quad C_4 = \sum_{k=1}^{N_P} \varepsilon_{11}^{(k)} r_{1k} h_{kP},$$

$$C_5 = \sum_{k=1}^{N_P} \frac{\varepsilon_{11}^{(k)} r_{1k}}{2} \left[(z_k^P)^2 - (z_{k-1}^P)^2 \right], \quad K_{1k}^2 = \frac{(d_{11}^{(k)})^2}{\varepsilon_{11}^{(k)} s_{P11}^{(k)}},$$

$$r_{1k} = \frac{d_{11}^{(k)}}{\varepsilon_{11}^{(k)} s_{P11}^{(k)}}. \tag{30}$$

We then combine Eqs. (22), (25), and (29) together for further use

$$\begin{cases} A\varepsilon - B\kappa - A_{01}E_0 - A_{02}H_0 = T_1 \\ B\varepsilon - D\kappa - C_1 E_0 - C_2 H_0 = M_1 \\ C_3 E_0 + C_4 \varepsilon - C_5 \kappa = D_1. \end{cases} \tag{31}$$

Note that ε, κ, E_0, and H_0 are function of x_1 and time t. These unknown functions should be determined using the motion equation of Eq. (3), Maxwell's equations of (4) and (5) and the boundary conditions on composite edges of $x_1 = \pm L$. From Eq. (31), we can see that if the coefficient $B \neq 0$, then the bending term κ can produce a tension T_1 and the strain ε can produce a bending moment M_1, in other words, the bending and longitudinal modes are coupled. These two modes can be decoupled only when $B = 0$.

IV. EQUATIONS OF MOTION IN THE THEORY OF LAMINATED MAGNETO-ELECTRO-ELASTIC BARS

The equations of motion in bar theory are obtained by integrating the three-dimensional equations of motion (3)–(5) over the bar thickness, i.e.,

$$\frac{\partial T_1}{\partial x_1} + X_1 = \rho \frac{\partial^2 u}{\partial t^2} - \tilde{\rho} \frac{\partial^3 w}{\partial x_1 \partial t^2} \tag{32a}$$

$$\frac{\partial Q}{\partial x_1} + X_3 = \rho \frac{\partial^2 w}{\partial t^2} \tag{32b}$$

$$Q = \frac{\partial M_1}{\partial x_1} - \tilde{\rho} \frac{\partial^2 u}{\partial t^2} - \tilde{\tilde{\rho}} \frac{\partial^3 w}{\partial x_1 \partial t^2}, \tag{32c}$$

where Q is a transverse shear stress in a cross sectional area of the composite; $X_1 = q_1^+ - q_1^-$; q_1^+ and q_1^- are the applied shear stresses to the top and bottom of the composite, respectively; $X_3 = q_3^+ - q_3^-$; q_3^+ and q_3^- are the applied normal stresses to the top and bottom of the composite, respectively, and

$$\rho = \sum_{k=1}^{N_P} h_{kP} \rho_{kP} + \sum_{k=1}^{N_M} h_{kM} \rho_{kM} + \sum_{k=1}^{N_E} h_{kE} \rho_{kE} \tag{33a}$$

$$\tilde{\rho} = \sum_{k=1}^{N_P} \frac{\rho_{kP}}{2} [(z_k^P)^2 - (z_{k-1}^P)^2] + \sum_{k=1}^{N_M} \frac{\rho_{kM}}{2} [(z_k^M)^2 - (z_{k-1}^M)^2]$$

$$+ \sum_{k=1}^{N_E} \frac{\rho_{kE}}{2} [(z_k^E)^2 - (z_{k-1}^E)^2] \tag{33b}$$

$$\tilde{\tilde{\rho}} = \sum_{k=1}^{N_P} \frac{\rho_{kP}}{3} [(z_k^P)^3 - (z_{k-1}^P)^3]$$

$$+ \sum_{k=1}^{N_M} \frac{\rho_{kM}}{3} [(z_k^M)^3 - (z_{k-1}^M)^3]$$

$$+ \sum_{k=1}^{N_E} \frac{\rho_{kE}}{3} [(z_k^E)^3 - (z_{k-1}^E)^3]. \tag{33c}$$

Note for static conditions that the time dependent terms are zero: in which case for $\frac{\partial}{\partial t} = 0$, the complete problem exactly divides into plane and bending problems. Dynamical equations (32) do not enable the complete system of equations for the theory of asymmetrical laminated electroelastic bars to be split into two decoupled systems for the tangential and transverse vibrations, as in the theory of bars of symmetrical structure. Using the constitutive relations (31) and the expressions $\varepsilon = \frac{\partial u(x_1,t)}{\partial x_1}$ and $\kappa = \frac{\partial^2 w(x_1,t)}{\partial x_1^2}$, the system of equations (32) can be expressed in terms of the displacements $u(x_1,t)$ and $w(x_1,t)$

$$
\begin{cases}
A\dfrac{\partial^2 u}{\partial x_1^2} - B\dfrac{\partial^3 u}{\partial x_1^3} = \rho\dfrac{\partial^2 u}{\partial t^2} - \tilde{\rho}\dfrac{\partial^3 w}{\partial x_1 \partial t^2} - X_1 \\[2mm]
B\dfrac{\partial^3 u}{\partial x_1^3} - D\dfrac{\partial^4 w}{\partial x_1^4} - \tilde{\rho}\dfrac{\partial^2 u}{\partial t^2} - \tilde{\tilde{\rho}}\dfrac{\partial^4 w}{\partial x_1^2 \partial t^2} = \rho\dfrac{\partial^2 w}{\partial t^2} - X_3.
\end{cases}
\tag{34}
$$

V. VIBRATIONS OF MULTILAYER ME COMPOSITES

Next, based on Eqs. (34), we will discuss some issues related to the bending-tension vibration of multilayer composites. The dynamic ME coefficient will be derived for free-free boundary condition at the edges of the composite. As a particular case, bi-layer composites made of ferromagnetic-ferroelectric will be considered.

As an example, consider the harmonic vibrations of a multilayer bar. The top and bottom surfaces are free of stresses, i.e., $q_i^{\pm} = 0$, ($i = 1,3$). We will assume that the system of equations (34) can be decomposed in to two systems of equations:

(A) The equations of the plane problem

$$
\begin{cases}
\dfrac{\partial^2 u_0}{\partial x^2} - \dfrac{\rho L^2}{A}\dfrac{\partial^2 u_0}{\partial t^2} = 0 \\[2mm]
T_{10} = \dfrac{A}{L}\dfrac{\partial u_0(x,t)}{\partial x} - A_{01}E_0 - A_{02}H_0,
\end{cases}
\tag{35}
$$

and (B) the equations of the bending problem

$$
\begin{cases}
\dfrac{\rho L^4}{D}\dfrac{\partial^2 w_0}{\partial t^2} + \dfrac{\partial^4 w_0}{\partial x^4} = 0 \\[2mm]
M_{10} = -\dfrac{D}{L^2}\dfrac{\partial^2 w_0(x_1,t)}{\partial x^2} - C_1 E_0 - C_2 H_0 \\[2mm]
Q_0 = \dfrac{1}{L}\dfrac{\partial M_{10}}{\partial x}.
\end{cases}
\tag{36}
$$

We next have to examine the following boundary conditions applied to the edges of the laminated composite. Both ends are free of stresses, i.e., at the edges, $x = \pm 1$ should satisfy

$$
T_{10} = 0, \quad Q_0 = 0 \text{ and } M_{10} = 0.
\tag{37}
$$

Using boundary conditions (37), the general solutions of Eqs. (35) and (36) can be obtained in the following form

$$
u_0(x,t) = e^{i\omega t}\frac{[A_{01}E_0 + A_{02}H_0]}{A\lambda_T}\frac{\sin(\lambda_T Lx)}{\cos(\lambda_T L)},
\tag{38}
$$

$$
w_0(x,t) = e^{i\omega t}\frac{C_1 E_0 + C_2 H_0}{D\lambda_B^2}\frac{1}{\cos(\lambda_B L) + \sin(\lambda_B L)cth(\lambda_B L)}
$$
$$
\times \left[\cos(\lambda_B Lx) - \frac{\sin(\lambda_B L)}{\text{sh}(\lambda_B L)}\cosh(\lambda_B Lx)\right].
\tag{39}
$$

For strain $\varepsilon = \frac{\partial u(x_1,t)}{\partial x_1}$ and bending $\kappa = \frac{\partial^2 w(x_1,t)}{\partial x_1^2}$, we can obtain the following representations

$$
\varepsilon = \tilde{\varepsilon}(x)e^{i\omega t}\frac{A_{01}E_0 + A_{02}H_0}{A}, \quad \kappa = \tilde{\kappa}(x)e^{i\omega t}\frac{C_1 E_0 + C_2 H_0}{D},
\tag{40a}
$$

where

$$
\tilde{\varepsilon}(x) = \frac{\cos(\lambda_T Lx)}{\cos(\lambda_T L)},
\tag{40b}
$$

$$
\tilde{\kappa}(x) = \frac{1}{\cos(\lambda_B L) + \sin(\lambda_B L)cth(\lambda_B L)}
$$
$$
\times \left[-\cos(\lambda_B Lx) + \frac{\sin(\lambda_B L)}{\text{sh}(\lambda_B L)}\cosh(\lambda_B Lx)\right].
\tag{40c}
$$

A. ME coefficient

Using open circuit conditions (12), along with solutions (38) and (39), we can drive the following compact expression for the ME coefficient α_{ME}

$$
\alpha_{ME} \equiv \alpha_{ME}(\omega) = -\frac{H_P}{H}\frac{\Delta_{0I}}{\Delta_{0II}};
\tag{41}
$$

where

$$
\Delta_{0I} = \frac{A_{02}C_4}{A}\frac{\text{tg}(\lambda_T L)}{\lambda_T L} + \frac{2C_2 C_5}{D}\Delta_0(\lambda_B L),
\tag{42}
$$

$$
\Delta_{0II} = C_3 + \frac{A_{01}C_4}{A}\frac{\text{tg}(\lambda_T L)}{\lambda_T L} + \frac{2C_1 C_5}{D}\Delta_0(\lambda_B L),
\tag{43}
$$

$$
\Delta_0(\lambda_B L) = \frac{\sinh(\lambda_B L)}{\sinh(\lambda_B L)\cos(\lambda_B L) + \sin(\lambda_B L)\cosh(\lambda_B L)}\frac{\sin(\lambda_B L)}{\lambda_B L}.
$$

For the case of ferromagnetic-ferroelectric bi-layer composites, the ME coefficient α_{ME} can be simplified as

$$
\alpha_{ME} \equiv \alpha_{ME}(\omega) = -\frac{q_{11}d_{11}}{s_{P11}\varepsilon_{11}}\frac{h_P}{h_P + h_m}\frac{\tilde{\Delta}_{0I}}{\tilde{\Delta}_{0II}};
\tag{44}
$$

where

$$
\tilde{\Delta}_{0I} = \frac{\gamma_0}{\gamma_0 + 1}\frac{\text{tg}(\lambda_T L)}{\lambda_T L} - \frac{3}{2}\frac{\gamma_1}{\gamma_2 + 1}\Delta_0(\lambda_B L).
\tag{45}
$$

$$
\tilde{\Delta}_{0II} = 1 - \text{K}_I^2 + \text{K}_I^2\frac{1}{\gamma_0 + 1}\frac{\text{tg}(\lambda_T L)}{\lambda_T L} + \frac{3}{2}\text{K}_I^2\frac{1}{\gamma_2 + 1}\Delta_0(\lambda_B L).
\tag{46}
$$

$$\lambda_T = \sqrt{\frac{\omega^2 \rho}{A}}, \quad \lambda_B = \sqrt[4]{\frac{\omega^2 \rho}{D}}, \quad \gamma_0 = \frac{s_{P11}}{s_{M11}} \frac{h_m}{h_p},$$

$$\gamma_1 = \frac{s_{P11}}{s_{M11}} \left(\frac{h_m}{h_p}\right)^2, \quad \gamma_2 = \frac{s_{P11}}{s_{M11}} \left(\frac{h_m}{h_p}\right)^3,$$

$$K_1^2 = \frac{d_{11}^2}{s_{P11}\varepsilon_{11}} \ .$$

1. Some notes and definitions

The frequency at which the ME coefficient $\alpha_{ME} \to \pm\infty$ is called the resonance frequency; whereas, the frequency at which $\alpha_{ME} \to 0$ is called the anti-resonance one. The resonance frequency can be determined from the equation $\Delta_{0II} = 0$. The anti-resonance frequency can be determined from the equation $\Delta_{0I} = 0$. The number of resonance and anti-resonant frequencies are discrete and infinite: i.e., the transcendental equations (42) and (43) (or (45) and (46) for bi-layer) have an infinite and discrete number of zeros.

2. Special cases

(A) **Static ME coefficient**. If we assume $\omega \to 0$ in Eqs. (41)–(43) or (44)–(46) for bi-layers, we can arrive to

$$\alpha_{ME} = \alpha_{ME}^S = -\frac{\dfrac{C_4 A_{02}}{A} + \dfrac{C_2 C_5}{D}}{C_3 + \dfrac{A_{01} C_4}{A} + \dfrac{C_1 C_5}{D}} \frac{H_P}{H}; \quad (47)$$

or to

$$\alpha_{ME} = -\frac{q_{11} d_{11}}{s_{P11}\varepsilon_{11}} \frac{h_P}{h_P + h_m} \left\{ \frac{\gamma_0}{\gamma_0 + 1} + \frac{1}{\Delta_{01}} [\gamma_1(\gamma_0 + 1) \right.$$
$$- \gamma_0(\gamma_1 - 1)] \left[\frac{\gamma_1 - 1}{\gamma_0 + 1} + 1 \right] \right\} \left\{ 1 - K_1^2 - K_1^2 \frac{1}{\Delta_{01}} [(\gamma_0 + 1) \right.$$
$$\left. + (\gamma_1 - 1)] \left[\frac{\gamma_1 - 1}{\gamma_0 + 1} - 1 \right] + K_1^2 \frac{1}{\gamma_0 + 1} \right\}^{-1}$$
$$\text{for bi} - \text{layers } \Delta_{01} = (\gamma_1 - 1)^2 - \frac{4}{3}(\gamma_0 + 1)(\gamma_2 + 1).$$
$$(48)$$

Formulae (47) is consistent to the model developed by Refs. 3–5 for static ME coefficient. In other words, assuming the vibration frequency approaches zero, from the formulae for dynamic ME coefficients, we can derive the static ME coefficient as a particular case.

(B) **Pure longitudinal mode:** If $D \to \infty$ in Eq. (41), we can obtain the dynamic ME coefficient for the pure longitudinal mode

$$\alpha_{ME} \equiv \alpha_{ME}(\omega)$$
$$= -\frac{H_P}{H} \frac{A_{02} C_4}{A} \frac{\text{tg}(\lambda_T L)}{\lambda_T L} \left\{ C_3 + \frac{A_{01} C_4}{A} \frac{\text{tg}(\lambda_T L)}{\lambda_T L} \right\}^{-1}. \quad (49)$$

Furthermore, similar conclusions can be derived for bi-layer composites: i.e., if in Eq. (44) $\gamma_2 + 1 \to \infty$, then one obtains a pure longitudinal mode

$$\alpha_{ME} \equiv \alpha_{ME}(\omega) = -\frac{q_{11} d_{11}}{s_{P11}\varepsilon_{11}} \frac{h_P}{h_P + h_m} \frac{\gamma_0}{\gamma_0 + 1} \frac{\text{tg}(\lambda_T L)}{\lambda_T L}$$
$$\times \left\{ 1 - K_1^2 + K_1^2 \frac{1}{\gamma_0 + 1} \frac{\text{tg}(\lambda_T L)}{\lambda_T L} \right\}^{-1}. \quad (50)$$

This case is consistent to the model developed in Refs. 22 and 23.

(C) **Pure bending mode:** If $A \to \infty$ in Eq. (41), we arrive at the dynamic ME coefficient for the pure bending mode, i.e.,

$$\alpha_{ME} \equiv \alpha_{ME}(\omega) = -\frac{H_P}{H} \frac{2 C_2 C_5}{D} \Delta_0(\lambda_B L)$$
$$\times \left\{ \frac{2 C_1 C_5}{D} \frac{\sinh(\lambda_B L)}{\sinh(\lambda_B L)\cos(\lambda_B L) + \sin(\lambda_B L)\cosh(\lambda_B L)} \frac{\sin(\lambda_B L)}{\lambda_B L} \right\}^{-1}; \quad (51)$$

and if $\gamma_0 + 1 \to \infty$ in Eq. (44), one has a pure bending mode for bi-layer structure, i.e.,

$$\alpha_{ME} \equiv \alpha_{ME}(\omega) = \frac{q_{11} d_{11}}{s_{P11}\varepsilon_{11}} \frac{h_P}{h_P + h_m} \frac{3}{2} \frac{\gamma_1}{\gamma_2 + 1} \Delta_0(\lambda_B L)$$
$$\times \left\{ 1 - K_1^2 + \frac{3}{2} K_1^2 \frac{1}{\gamma_2 + 1} \Delta_0(\lambda_B L) \right\}^{-1}. \quad (52)$$

VI. NUMERICAL RESULTS

To demonstrate the validity of the theory, we will consider bi-layer laminate composites. In the calculations, we will use the following material parameters for Metglas-PZT composite bilayers given in Table I. For numerical illustrations, the Metglas-PZT bilayer composite was chosen, as a model system, because it has higher piezoelectric and piezomagnetic coefficients.

A. Theoretical validations and experimental verifications

1. Sensor fabrication

To check the theoretical developments, we performed two experiments using Metglas-PZT bi-layer composites. In the first experiment, we assumed a laminate length of $2L = 8 \cdot 10^{-2}$ m and in the second $2L = 4 \cdot 10^{-2}$ m. The maximum number of Metglas layer was chosen as 21. To fabricate bi-layer Metglas-PZT laminates, we obtained commercially available PZT fibers from Smart Materials (Florida, USA) and Metglas foils from Vitrovac Company (Germany). First of all, 5 pieces of $180\,\mu m$ thick PZT fibers were oriented

TABLE I. Material parameters (compliance coefficient's $(10^{-12}\text{m}^2/\text{N})$, piezomagnetic coupling $q(10^{-12}\text{m/A})$, piezoelectric coefficient $d(10^{-12}\text{m/V})$, density $\rho(\text{kg/m}^3)$, permeability μ, and permittivity ε for lead zirconate titanate (PZT) and Metglass.

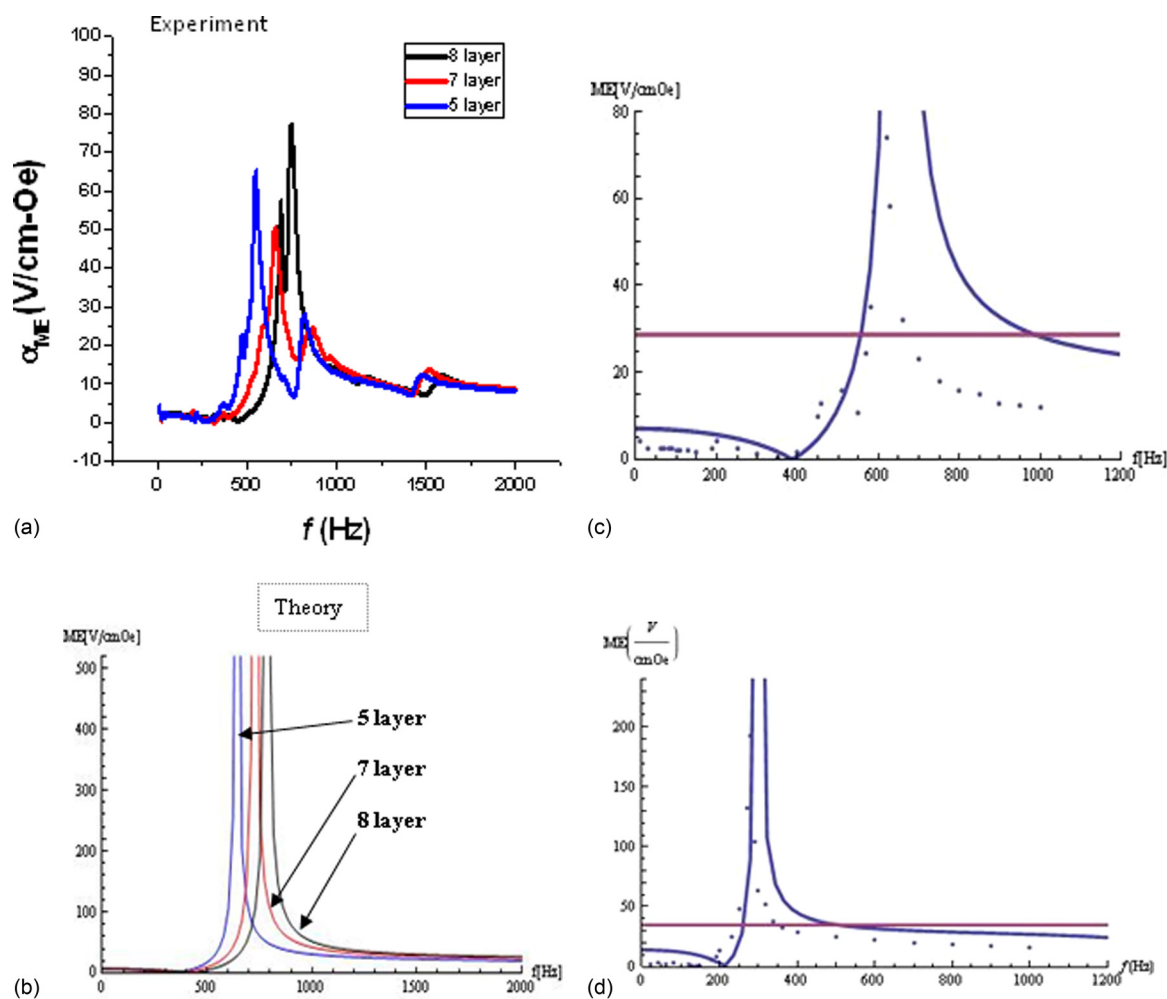| Materials	s_{11}	s_{12}	s_{13}	s_{33}	q_{11}	q_{13}	d_{13}	d_{11}	μ_{11}/μ_0	$\varepsilon_{11}/\varepsilon_0$	ρ
PZT	15.3	−5	−7.22	17.3			−175	400	1	1750	7600
Metglass	10				50000				45000		7180

FIG. 3. ME voltage coefficient as a function of $f = \omega/2\pi$. Results are for a PZT-Metglass bilayer. Length of the composite $2L = 44 \cdot 10^{-2}$ m; Thickness of PZT is $h_P = 1.8 \cdot 10^{-4}$ m; thickness of one layer of Metglas is $h_M = 2.5 \cdot 10^{-5}$ m. (b) ME voltage coefficient as a function of $f = \omega/2\pi$. Results are for a PZT-Metglass bilayer. Length of the composite $2L = 4 \cdot 10^{-2}$ m; Thickness of PZT is $h_P = 1.8 \cdot 10^{-4}$ m; thickness of one layer of Metglas is $h_M = 2.5 \cdot 10^{-5}$ m. (c) ME voltage coefficient as a function of $f = \omega/2\pi$. Comparison of ME voltage coefficient based on the Eq. (44) for bending-tension coupled model (blue line) and on the Eq. (52) for pure longitudinal mode (purple line). Results are for a PZT-Metglass bilayer. Number of Metglas layers $N = 4$. Length of the composite $2L = 4 \cdot 10^{-2}$ m; Thickness of PZT is $h_P = 1.8 \cdot 10^{-4}$ m; (d) ME voltage coefficient as a function of $f = \omega/2\pi$. Comparison of ME voltage coefficient based on the Eq. (44) for bending-tension coupled model (blue line) and on the Eq. (52) for pure longitudinal mode (purple line). Results are for a PZT-Metglass bilayer. Number of Metglas layers $N = 12$. Length of the composite $2L = 8 \cdot 10^{-2}$ m; Thickness of PZT is $h_P = 1.8 \cdot 10^{-4}$ m; thickness of one layer of Metglas is $h_M = 2.5 \cdot 10^{-5}$ m. Dots are experimental results.

along the long axes to form a piezoelectric layer that was in total one cm wide and 4 cm long. Two Interdigited (ID) Kapton®-based electrodes were then bonded to the top and bottom surfaces of the PZT layer in a multi push-pull mode configuration. Various layers of Metglas foils of 8 cm in length (or 4 cm in length) and 1 cm in width were bonded together first, and subsequently laminated to only one side of PZT layer of 4 cm in length to achieve the bi-layer structure.

B. Result and discussion

The ME voltage coefficients α_{ME} for bending mode laminates with different layers of Metglas were measured as a function of frequency of ac magnetic driving field. A commercial lock-in amplifier (SR-850) was used to drive a pair of Helmholtz coils, which can generate an ac magnetic field of $H_{ac} = 0.1$ Oe over a frequency range of 10 Hz $< f = \omega/2\pi < 2$ kHz. The induced voltage from the ME laminates was measured by this amplifier as well. Figure 3(a) shows

how α_{ME} was affected by the number of Metglas layers. The peak positions exhibited significant tenability on changing the number (N) of Metglas layers. For 4 cm (Metglas length), the resonant frequency shifted from 325 Hz to 790 Hz with N = 1 to N = 8. Bending mode laminates with N = 4 showed a maximum value of $\alpha_{ME} > 100$ V/cm-Oe. In Figures 3(a) (experiment) and 3(b) (predicted, based on formulae (44)), the ME voltage coefficient α_{ME} is shown as a function of ac magnetic field frequency $f = \omega/2\pi$. The length of the composite was $2L = 4 \cdot 10^{-2}$ m; the thickness of PZT was $h_P = 1.8 \cdot 10^{-4}$ m; and the thickness of each Metglas layer was $h_M = 2.5 \cdot 10^{-5}$ m.

Figure 3(a) shows the experimental results for different layers (number of layers = 5;7;8), and Figure 3(b) shows the theoretical validations using the same parameter choice. As can be clearly seen from these two figures, the experimental data and theoretical predictions are consistent not only qualitatively but also quantitatively. For example, the values of the resonant frequency from experiment differed only
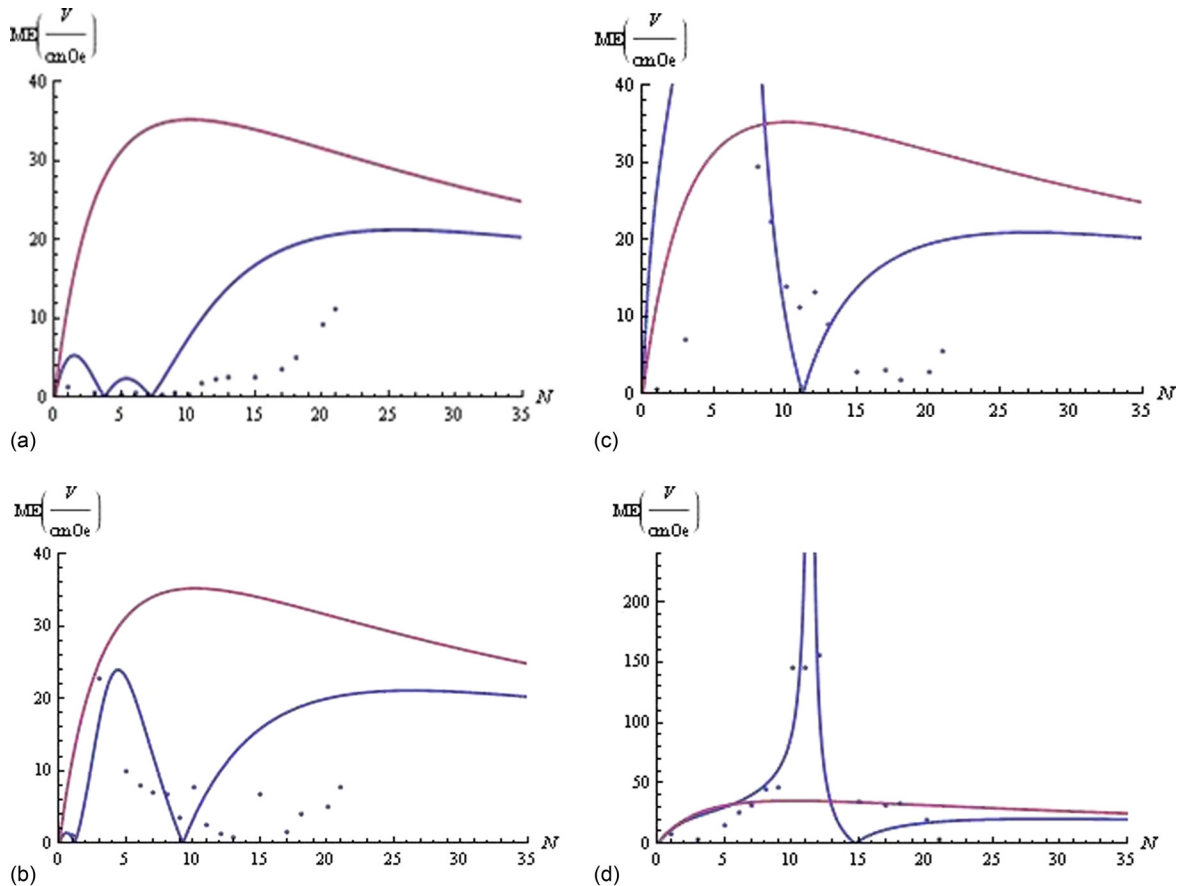
FIG. 4. ME voltage coefficient as a function of N number of layers of Metglas. Frequency value $f = 110\,\text{Hz}$. Comparison of ME voltage coefficient based on the Eq. (44) for bending-tension coupled model (blue line) and on the Eq. (52) for pure longitudinal mode (purple line). Results are for a PZT-Metglass bilayer. Length of the composite $2L = 8 \cdot 10^{-2}\,\text{m}$; Thickness of PZT is $h_P = 1.8 \cdot 10^{-4}\,\text{m}$; thickness of one layer of Metglas is $h_M = 2.5 \cdot 10^{-5}\,\text{m}$. Dots are experimental results. (b) ME voltage coefficient as a function of N number of layers of Metglas. Frequency value $f = 150\,\text{Hz}$. Comparison of ME voltage coefficient based on the Eq. (44) for bending-tension coupled model (blue line) and on the Eq. (52) for pure longitudinal mode (purple line). Results are for a PZT-Metglass bilayer. Length of the composite $2L = 8 \cdot 10^{-2}\,\text{m}$; Thickness of PZT is $h_P = 1.8 \cdot 10^{-4}\,\text{m}$; thickness of one layer of Metglas is $h_M = 2.5 \cdot 10^{-5}\,\text{m}$. Dots are experimental results. (c) ME voltage coefficient as a function of N number of layers of Metglas. Frequency value $f = 200\,\text{Hz}$. Comparison of ME voltage coefficient based on the Eq. (44) for bending-tension coupled model (blue line) and on the Eq. (52) for pure longitudinal mode (purple line). Results are for a PZT-Metglass bilayer. Length of the composite $2L = 8 \cdot 10^{-2}\,\text{m}$; Thickness of PZT is $h_P = 1.8 \cdot 10^{-4}\,\text{m}$; thickness of one layer of Metglas is $h_M = 2.5 \cdot 10^{-5}\,\text{m}$. Dots are experimental results. (d) ME voltage coefficient as a function of N number of layers of Metglas. Frequency value $f = 280\,\text{Hz}$. Comparison of ME voltage coefficient based on the Eq. (44) for bending-tension coupled model (blue line) and on the Eq. (52) for pure longitudinal mode (purple line). Results are for a PZT-Metglass bilayer. Length of the composite $2L = 8 \cdot 10^{-2}\,\text{m}$; Thickness of PZT is $h_P = 1.8 \cdot 10^{-4}\,\text{m}$; thickness of one layer of Metglas is $h_M = 2.5 \cdot 10^{-5}\,\text{m}$. Dots are experimental results.

slightly with the theoretical predictions. In addition, the spectra of α_{ME} computed using our model showed only discrete resonances (see Fig. 3(b)). Please bear in mind that real structures always exhibit losses, which are related primarily to nonideal contacts or introduction of dielectric and magnetic losses in the permittivity and permeability tensors (see Fig. 3(a)). These losses determine the resonance line width and limit the peak value of α_{ME}. In reality, such dissipation effects should be included in the modeling to quantitatively compare with experimental spectra. In this paper, we outlined qualitative effects in ME composites, and losses (damping effects) were not taken into consideration. However, losses could be taken into account in the modeling: for example, in formulas (41)–(52), the frequency ω could be represented as a complex quantity, then the imaginary part of ω would introduce the damping coefficient.

In Figures 3(c) and 3(d), we represent experimental and theoretical results in the same graph for α_{ME} as a function of $f = \omega/2\pi$. Comparisons of α_{ME} based on Eq. (44) for the

bending-tension coupled model (blue line) and on Eq. (52) for the pure longitudinal mode (purple line) is given in this figure, where dots are experimental results. In Figure 3(c), we show the case where number of Metglass layers $N = 4$ and length of the composite $2L = 4 \cdot 10^{-2}\,\text{m}$. In Figure 3(d), we show the case when number of Metglass layers $N = 12$ and length of the composite $2L = 8 \cdot 10^{-2}\,\text{m}$. Thickness of one layer of Metglas is $h_M = 2.5 \cdot 10^{-5}\,\text{m}$. From these two figures, one can clearly see that the bending-tension coupled model much better describes the experimental result, relative to the theory based on a pure longitudinal mode.

In Figures 4(a)–4(d), we show α_{ME} as a function of N. Comparisons of α_{ME} based on Eq. (44) for the bending-tension coupled model (blue line) and on Eq. (52) for the pure longitudinal mode (purple line) are shown, where dots again represent experimental data. The length of the composite was $2L = 8 \cdot 10^{-2}\,\text{m}$, the thickness of PZT layer was $h_P = 1.8 \cdot 10^{-4}\,\text{m}$, and the thickness of each Metglas layer was $h_M = 2.5 \cdot 10^{-5}\,\text{m}$. The values of the frequencies were
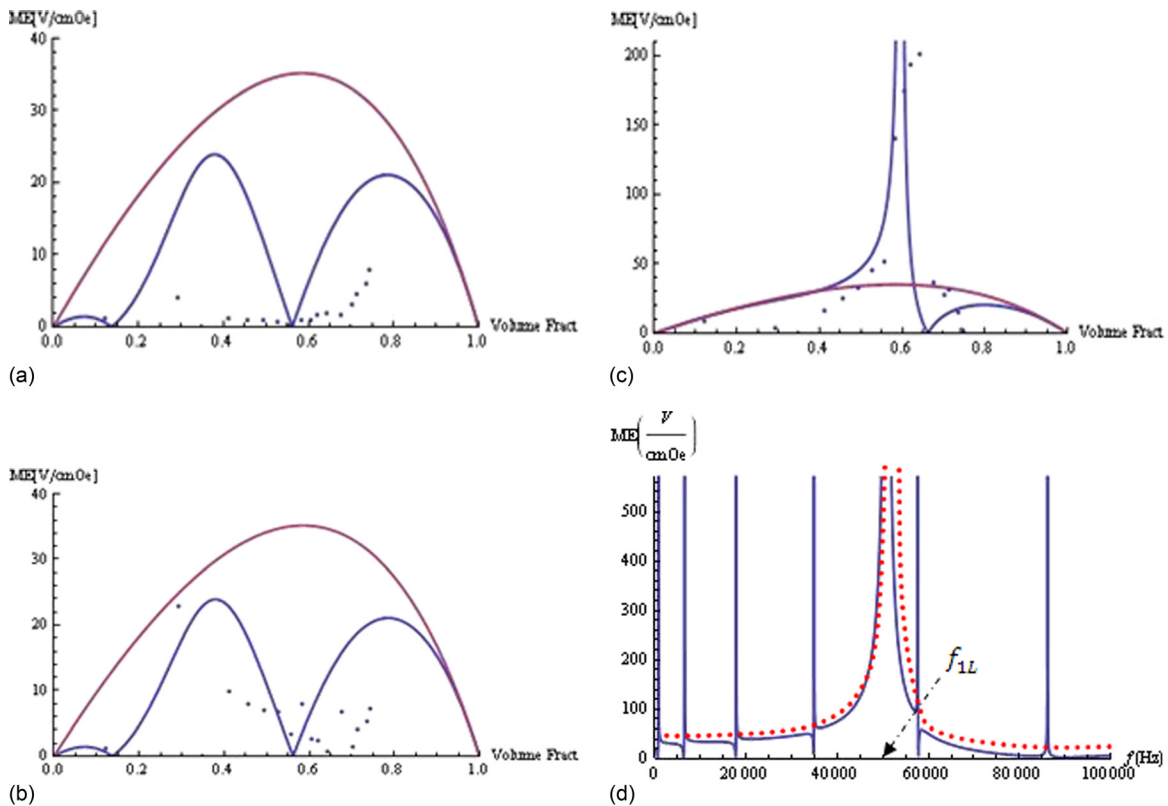
FIG. 5. Low-frequency ME voltage coefficient as a function of bilayer volume fraction. Comparison between the theory and experiment dates (dots). Solid blue line based on Eq. (44) (bending-tension coupled mode) and purple line based on Eq. (52) (only longitudinal mode). Data presented for Metglas-PZT bilayer for frequency value $f = 120$ Hz, 2 L = 8 cm. (b) Low-frequency ME voltage coefficient as a function of bilayer volume fraction. Comparison between the theory and experiment dates (dots). Solid blue line based on Eq. (44) (bending-tension coupled mode) and purple line based on Eq. (52) (only longitudinal mode). Data presented for Metglas-PZT bilayer for frequency value $f = 150$ Hz, 2 L = 8 cm. (c) Low-frequency ME voltage coefficient as a function of bilayer volume fraction. Comparison between the theory and experiment dates (dots). Solid blue line based on Eq. (44) (bending-tension coupled mode) and purple line based on Eq. (52) (only longitudinal mode). Data presented for Metglas-PZT bilayer for frequency value $f = 280$Hz, 2L = 8 cm. (d) ME voltage coefficient as a function of $f = \omega/2\pi$. Results are for a PZT-Metglass bilayer. The value of $h_P/L = 0.01$, $h_M/L = 0.02$. Pure longitudinal mode is shown as a red dotted line.

$f = \omega/2\pi = 110$ Hz (see Fig. 4(a)), $f = \omega/2\pi = 150$ Hz (see Fig. 4(b)), $f = \omega/2\pi = 200$ Hz (see Fig. 4(c)), and $f = \omega/2\pi = 280$ Hz (see Fig. 4(d)). In each of these cases, the bending-tension coupled model showed better correlation with experimental data than a theory based on a pure longitudinal mode. In particular, the bending-tension theory was in much better agreement with experiments near the resonant frequencies (see Fig. 4(d) for $f = \omega/2\pi = 280$ Hz).

Finally, the values of α_{ME} at different frequencies are given in Figures 5(a)–5(c), which show data for volume ratio effect of Metglas on α_{ME}. The low-frequency value of α_{ME} is shown as a function of bilayer volume fraction. In Figures 5(a)–5(c), we compare predicted and experimental values. The solid blue line is based on Eq. (44) (bending-tension coupled mode), the purple line is based on Eq. (52) (only longitudinal mode), and the dots are the experimental data. The data presented were for Metglas-PZT bilayers of length 2L = 8 cm for following frequency values: $f = 120$ Hz (Fig. 5(a)); $f = 150$ Hz (Fig. 5(b)); $f = 280$ Hz (Fig. 5(c)). It can be seen that α_{ME} did not show a similar volume ratio effect as predicted by the theoretical model that only considered longitudinal deformations.[4,14,23] Clearly from this figure, we can also see that the bending-tension coupled mode is in much better agreement with experimental data than longitudinal mode. In Fig. 5(d), we can see that overall the value of the ME coefficient increased upon approaching the first reso-

nance frequency of the pure longitudinal mode f_{1L}: above which frequency, the overall behavior resembled that of the longitudinal mode (pure longitudinal mode is shown as a red dotted line). However, before approaching the first resonance frequency of the pure longitudinal mode f_{1L}, the ME coefficient exhibited resonances at the bending mode frequencies.

VII. DISCUSSIONS

A dynamic theory for arbitrary laminated magneto-electro-elastic bars was constructed. A theoretical model including both bending and longitudinal vibration effects was developed for predicting the magneto electric (ME) effects in laminated bar composite structures consisting of magnetostrictive, piezoelectric, and pure elastic layers. Analytical expressions indicate that the vibration frequency strongly influenced the strain distribution in the laminates and that these effects in turn strongly influenced the ME coefficients. As particular cases, the low frequency ME and dynamic coefficients were derived. Dynamic ME coefficients were also derived. As a demonstration, the developed theory for multilayer ME composites was applied to ferromagnetic-ferroelectric bilayers. The vibration of a two-layer magneto-electro-elastic bar was considered. The displacements, stresses, and magneto-electrical quantities were calculated, and the dependence of the coupling coefficient on the

vibration frequencies and the ferromagnetic/piezoelectric layer thickness studied. As a particular case, a theoretical model was presented for low-frequency ME effects in bilayers. We considered boundary condition corresponding to that which is free to vibrate at both ends.

As a demonstration, our theory for multilayer ME composites was then applied to ferromagnetic-ferroelectric bilayers. The model was applied to a specific case of Metglas-PZT bilayers. A theoretical model was presented for static (low-frequency) ME effects in bilayers as a particular case. We analyzed the influence of Metglas geometry (length, thickness) and Metglas/PZT volume fraction on the ME coefficient. We performed experiments for Metglas-PZT bilayers. The frequency dependence of the ME coefficient was also presented for different geometries (length, thickness) of Metglas. The theory shows good agreement with experimental data, even around the resonance frequency.

ACKNOWLEDGMENTS

[1]M. Fiebig, J. Phys. D: Appl. Phys. **38**, R123 (2005).
[2]C. W. Nan, M. I. Bichurin, S. X. Dong, D. Viehland, and G. Srinivasan, J. Appl. Phys. **103**, 031101 (2008).
[3]G. Harshe, J. P. Dougherty, and R. E. Newnham, Int. J. Appl. Electromagn. Mater. **4**, 145 (1993).
[4]M. I. Bichurin, V. M. Petrov, S. V. Averkin, and E. Liverts, J. Appl. Phys. **107**, 053904 (2010).
[5]C.-M. Chang and G. Carman, Phys. Rev. B **76**, 134116 (2007).
[6]W. Q. Chen, Y. Y. Zhou, C. F. Lu, and H. J. Ding, Eur. J. Mech. A/Solids **28**, 720 (2009).
[7]V. M. Petrov, M. I. Bichurin, V. V. Zibtsev, S. K. Mandal, and G. Srinivasan, J. Appl. Phys. **106**, 113901 (2009).
[8]J. Gao, Y. Shen, Y. Wang, P. Finkel, J. Li, and D. Viehland, IEEE Trans. Ultrason. Ferroelectr. Freq. Control **58**, 1545 (2011).
[9]M. Guo and S. Dong, IEEE Trans. Ultrason. Ferroelectr. Freq. Control **56**, 2578 (2009).
[10]Z. P. Xing, S. X. Dong, J. Y. Zhai, L. Yan, J. F. Li, and D. Viehland, Appl. Phys. Lett. **89**, 112911 (2006).
[11]D. V. Chashin, Y. K. Fetisov, K. E. Kamentsev, and G. Srinivasan, Appl. Phys. Lett. **92**, 3 (2008).
[12]V. M. Petrov, G. Srinivasan, M. I. Bichurin, and T. A. Galkina, J. Appl. Phys. **105**, 6 (2009).
[13]D. Hasanyan, Y. J. Wang, J. Q. Gao, M. H. Li, J. F. Li, and D. Viehland, Phys Rev B (submitted).
[14]Y. K. Fetisov, D. V. Chashin, A. G. Segalla, and G. Srinivasan, J. Appl. Phys. **110**, 066101 (2011).
[15]G. Sreenivasulu, S. K. Mandal, S. Bandekar, V. M. Petrov, and G. Srinivasan, Phys. Rev. B **84**, 144426 (2011).
[16]J. Gao, J. Das, Z. Xing, J. Li, and D. Viehland, J. Appl. Phys. **108**, 084509 (2010).
[17]S. V. Gopinathan, V. V. Varadan, and V. K. Varadan, Smart Mater. Struct **9**, 24 (2000).
[18]N. N. Rogacheva, J. Appl. Math. Mech **74**, 721 (2010).
[19]V. Z. Parton and B. A. Kudryavtsev, *Electromagnetoelasticity: Piezoelectricsand Electrically Conductive Solids* (Gordon and Breach Science, New York, 1988).
[20]H. F. Tiersten, *Linear Piezoelectric Plate Vibrations* (Plenum, New York, 1969).
[21]H. S. Tzou, *Piezoelectric Shells: Distributed Sensing and Control of Continua* (Kluwer Academic, 1993).
[22]D. A. Filippov, M. I. Bichurin, C. W. Nan, and J. M. Liu, J. Appl. Phys. **97**, 4 (2005).
[23]D. A. Filippov, M. I. Bichurin, V. M. Petrov, V. M. Laletin, N. N. Poddubnaya, and G. Srinivasan, Tech. Phys. Lett. **30**, 6 (2004).